NUMERICAL MODELLING OF THE INTERACTION BETWEEN BRINE-NCG SOLUTIONS AND GREYWACKE

Dale Emet Altar[1,2], Eylem Kaya[1]

[1]University of Auckland, Auckland, New Zealand

[2] Philippine Geothermal Production Company Inc., 14/F 6750 Building Ayala Avenue, Makati City, Philippines

dalt507@aucklanduni.ac.nz

Keywords: *Carbon dioxide, hydrogen sulphide, NCG, co-injection, TOUGHREACT, modelling, brine, fluid-rock interaction, chemical kinetics*

ABSTRACT

Global warming as an impact of human activities is a widely accepted theory. It is imperative that greenhouse gas (GHG) emissions be reduced as early as is practicable, especially in the energy production sector. For the geothermal power sector, it is important to explore alternative disposal technologies for GHG emissions in place of the common practice of releasing the separated non-condensable gases (NCG) into the atmosphere.

One alternative which has received widespread focus is geologic sequestration, or the injection of NCG deep into the earth. Co-injection of NCG with the reinjected fluids (i.e. brine and condensate) is considered a prime option compared to supercritical injection.

Another potential impact of the co-injection of NCG is pH-lowering which may lead to reservoir permeability stimulation. In theory, the increased acidity of the resulting solution will dissolve minerals in the formation, improving permeability, or even creating new permeability zones over time.

GNS Science conducted a series of experiments on the interaction of brine with greywacke. In 2015, Passarella et al. simulated the interaction between brine with dissolved CO_2 and H_2S, and a sample of greywacke from the Waotu quarry in South Waikato. To investigate the physicochemical processes of NCG-brine-reservoir rock interaction and quantify the effect of NCG on petro-physical properties of geothermal reservoirs it is necessary to carry out numerical simulations.

This work aimed to simulate the results from the experiments of Passarella et al. (2015) with the use of TOUGHREACT. The goal of the study is to develop numerical simulation techniques to model and understand the effects of the reinjection of brine with dissolved NCG. The resulting model provided insights into the geochemical behaviour of greywacke-brine-NCG under reservoir conditions and impacts of this interaction on permeability and porosity. The numerical simulation also assesses the evolution of mineral reactive surface areas as a result of the degree of dissolution and injection flow rate, and investigates the potential for NCG sequestration.

1. INTRODUCTION

In February 2018, NASA recorded the CO_2 level in the atmosphere at 408 ppm. This value is expected to increase as an effect of human industrial practices. Based on the work by Solomon et al. (2008) should CO_2 levels rise to 450 ppmv in the atmosphere, global temperatures can elevate by 1.4 °C compared to pre-industrial conditions; by 1.9 °C at 550 ppmv; and by 2.4 °C at 650 ppmv. Arresting the further increase of greenhouse gas concentrations in the atmosphere should then be a critical global goal in order to prevent future unmitigable consequences of climate change.

Globally, the energy production sector accounts for 78% of greenhouse gas emissions according to 2013 data (Stats NZ, 2018). The power generation sector then presents opportunities for the reduction of greenhouse gas emissions. Shifting from thermal power generation technologies to renewables like geothermal, hydropower, wind or solar is a step forward in the goal of greenhouse gas reduction.

Geothermal plants produce CO_2 at a rate of 122 tonnes per GWh, only a factor of 0.14 of the contribution from coal, and 0.24 compared to natural gas according to a 2016 report by Fridriksson et al. for the World Bank. However based on the figures from the report "Comparison of Lifecycle Greenhouse Gas Emissions of Various Electricity Generation Sources" by the World Nuclear Association (2011), greenhouse gas emissions from geothermal power is still 4.7 times that from hydroelectric or wind, and 4.2 times that from nuclear power. These figures present an opportunity to further reduce CO_2 emissions related to geothermal power production.

The production of CO_2 and other NCGs like H_2S, H_2, NH_3 and CH_4 cannot be avoided as they occur naturally within hydrothermal systems. It is therefore important to explore alternative disposal technologies for GHG emissions.

One alternative which has received focus in the geothermal industry is geologic sequestration. In the oil and gas industry, injection of supercritical CO_2 into saline aquifers and depleted reservoirs has been widely studied, modelled and implemented, for example, in the works of Knauss et al. (2005), Kaszuba et al. (2003) and Doughty et al. (2001).

Parallel efforts have been made for the geothermal industry. Co-injection of NCG with the reinjected fluids (i.e. brine and condensate) is considered a prime option compared to supercritical injection. From a capital expenditure and operational point of view, co-injection eliminates the need for more sophisticated compression equipment to reach supercritical conditions, as well as the requirement to drill a dedicated injection well, which for the relatively small volume of NCG can prove cost-prohibitive.

Dissolution of NCGs with the brine (or condensate) may also lead to favourable changes in injectate chemistry. For example in a representative system, for every kg of brine produced for reinjection, 0.0033 kg of CO_2 and 0.0003 kg of H_2S are vented to the atmosphere from the steam. If we

dissolve the NCGs back into the brine, they will cause a shift in the fluid pH, as shown in Figure 1.

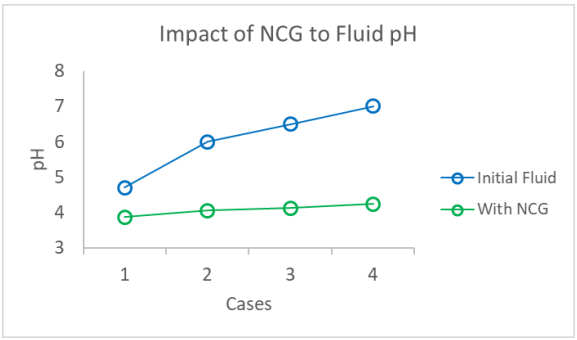

Figure 1: pH impact of dissolving NCG into produced brine in at various starting pH values

Note how the pH is expected to shift to values of approximately 4 from any starting point pH between 4.5 and 7. One positive impact of this shift in pH is to slow down the formation of amorphous silica during the process of reinjection. Another potential impact of this shift in pH is reservoir permeability stimulation. In theory, the acidity of the resulting solution will dissolve minerals in the formation, improving permeability, or even creating new permeability zones over time.

To further the understanding of the latter impact of NCG mixing with injectate, GNS Science conducted a series of experiments on the interaction of brine with greywacke, which represents the basement formation in the Taupo volcanic zone in which most brines are reinjected. In 2015, GNS Science simulated the interaction between brine with dissolved CO_2 and H_2S, and a sample of greywacke from the Waotu quarry in South Waikato. Based on the experiment report (Passarella et al., 2015), at 200°C, corrosion of ferromagnesian and chlorite mineralisation became predominant, with the concurrent precipitation of pyrite and clay minerals. A schematic of the experimental apparatus is shown in Figure 2.

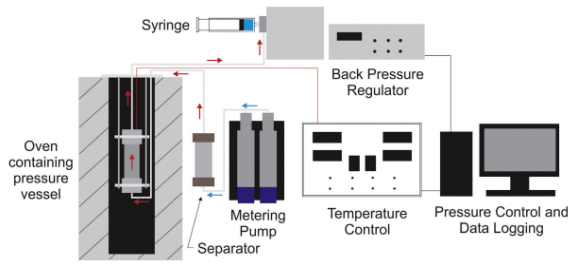

Figure 2: Schematic diagram of the reactor equipment used for the brine-NCG and greywacke interaction simulation. Reprinted from Sonney & Mountain (2013).

Numerical modelling of the trapping mechanism for the NCGs have also been the topic of multiple scientific works. In past studies, modelling was performed primarily using applications within the TOUGH suite.

In the work by Kaya & Zarrouk (2017), the trapping mechanism was represented in the adsorption behaviour of CO_2-H_2S-water mixtures, though the chemical reactions between the fluid and the reservoir rocks were not considered in the study. Their results show that in certain conditions, the NCG co-injection can improve steam rates in the short term, but that injection strategies must be formulated specifically to prevent premature breakthrough of NCGs into the production which will increase the NCG removal load topside.

In the study by Xu et al. (2005), TOUGHREACT was employed to incorporate reactive geochemical processes into the model. TOUGHREACT is a "numerical simulation program for chemically reactive non-isothermal flows of multiphase fluids in porous and fractured media, developed by introducing reactive chemistry into the multiphase flow code TOUGH2" (Lawrence Berkeley National Laboratory, 2018). A key finding in their study is that minerals may dissolve closer to the injection point as an impact of the lower pH, but as radial distance extends from the injection point equilibrium between the fluid and the minerals can be reached such that no further dissolution (or precipitation) occurs. It is also important to note that the chemical trapping of CO_2 upon precipitation of secondary carbonates will reduce porosity and permeability.

The goal of this work is to develop numerical simulation techniques to model and understand the effects of the reinjection of brine or condensate with dissolved non-condensable gases, primarily CO_2 and H_2S. Detailed transient reactive transport numerical models (by using TOUGH2 and TOUGHREACT) were developed to understand the impact of the injected NCGs on fluid-rock interactions.

2. METHODOLOGY

2.1 Experimental Set-up

To understand the chemical reactions that occur between brine with dissolved NCGs and reservoir rocks, Passarella et al. (2015) of GNS Science conducted a simulated fluid-rock interaction experiment. The first component of the experiment was Manaia Hill greywacke samples from the Waotu quarry. Greywacke samples were crushed and sieved to get particles of 355 to 500 µm in size. The total sample mass used was 23.7 grams, placed inside a titanium pressure vessel with a height of 15 cm and a radius of 0.625 cm. For the samples used no petrological analysis was done, but GNS Science was able to provide modal analysis for similar Manaia Hill formation samples from the development of the Karapiro Dam, located 40 km from the Waotu quarry, and from the Tongariro hydroelectric development (Palmer et al., 1995).

The modal analysis data was reviewed and reinterpreted into mineral fractions that will be useful for the model. Minerals identified in the paper by Passarella et al., both primary and secondary, were used to ground the interpretation. The resulting mineralogy and volume fractions can be found in Table 1.

The second component of the experiment is the brine and NCG sample. Low-pressure separator brine obtained from a power station in New Zealand was deoxygenated and used.

Before experimental runs, approximately 800 ml of brine was combined with approximately 200 ml of NCG mix. The NCG mix was supplied from a 6.2 barg external tank and contained 96%w CO_2, 4%w H_2S and 0.1%w H_2. Pressure was exerted on the combined volume inducing the dissolution of the gas. No vapour phase remained after the dissolution process. NCG and brine mixing was done twice

during the experiment, the second time to refill the brine supply. Unfortunately, sample analysis was not done on either batch of the brine-NCG solutions after gas dissolution. It therefore became necessary to predict the resulting brine chemistry.

Table 1: Mineralogy and volume fractions in the greywacke sample as interpreted for use with TOUGHREACT

Mineral	% Vol
Pyrite	0.3%
Quartz	20.3%
Amorphous Silica	0.0%
Chlorite	0.5%
Illite	0.5%
Calcite	2.8%
Albite	23.1%
K-Feldspar	1.9%
Augite	0.2%
Anhydrite	0.1%
Smectite-Ca	0.0%
Siderite	0.0%
Inert	51.0%
Total	100%

2.2 Brine-NCG Chemistry Prediction

The chemistry of the brine mixture after the addition of NCG was simulated using TOUGHREACT. A static model with only 800 ml of total volume (to represent the accumulator) and a single pore fluid composition was created. In the experiment, a finite volume of gas was added and was observed to dissolve in the solution fully. It is then prudent to model the gas dissolution as the addition of a fixed amount of gas molecules in aqueous form to the brine.

To do this, first, the total NCG molar input was calculated. According to Passarella (Personal communications, 2018), both the brine and gas volumes were not exactly measured during brine preparation. Through trial models, it was found that a volume of 180 ml of gas mixed with 800 ml of brine gave the best match for CO_2 content in the experiment samples. Using the volume of 180 ml at 20 °C and 7.2 bara pressure, total component gas mole counts were calculated.

In TOUGHREACT, CO_2(aq), H_2S(aq) and H_2(aq) were added as primary aqueous components, along with HCO_3^- and HS^-. In this case, TOUGHREACT does not automatically calculate the equilibrium state between primary aqueous species. For the system to reach equilibrium, parameters for aqueous kinetics between the species were used. For example, the equilibrium for dissolved CO_2 was modelled using the reaction as described in Equation 1. The parameters k_1 and k_{-1} pertain to the forward and reverse reaction rate constants. The same was done for H_2S.

$$CO_{2(aq)} \underset{k_{-1}}{\overset{k_1}{\rightleftharpoons}} HCO_3^- + H^+ \qquad \textbf{Equation 1}$$

Both the initial water chemistry and the output chemistry from the model are presented in Table 2. Note the decrease in pH and the changes to the concentrations of CO_2(aq), HCO_3^-, H_2S(aq) and HS^-. The model chemistry output served as the chemistry input to the reactor model.

Table 2: Initial Water and resulting Mixing Model chemistry profiles. All concentrations are in mol/kg.

Chemical Species	Initial Water	Mixed Model
pH	4.7	3.9
Na^+	3.2214E-02	3.2214E-02
K^+	5.4544E-03	5.4544E-03
Ca^{2+}	9.4810E-05	9.4810E-05
Mg^{2+}	4.7859E-06	4.7859E-06
Fe^{2+}	1.5275E-05	1.5275E-05
Al^{3+}	3.3052E-05	3.3052E-05
Cl^-	3.3962E-02	3.3962E-02
HCO_3^-	1.6444E-08	4.3777E-05
SO_4^{2-}	9.8184E-04	9.8184E-04
SiO_2(aq)	1.7876E-02	1.7876E-02
As	4.3472E-05	4.3472E-05
B(aq)	3.3714E-03	3.3714E-03
Li^+	1.3966E-03	1.3966E-03
Mn^{2+}	1.4118E-06	1.4118E-06
CO_2(aq)	6.4184E-02	6.4140E-02
H_2S(aq)	3.4493E-03	3.4421E-03
H_2(aq)	1.4596E-04	1.4596E-04
HS-	3.036E-08	7.2624E-06

2.3 Reactor Model

The Reactor Model required declarations for both the fluid chemistry profiles and the mineral zones. Additionally, the kinetic and equilibrium parameters for the dissolution and precipitation of minerals had to be defined. Data for each mineral were referenced from various literature sources.

Mineral dissolution rate constants were primarily adapted from the report by Palandri & Kharaka (2004). Precipitation rate constants were derived using the forward dissolution rate constant and the equilibrium constant for the reaction following the relationship theorem as reported by Horiuti (1956), which is an expansion of the classical theorem for a typical reaction which occurs in one step. The relationship is shown in Equation 2.

$$\frac{k_+}{k_-} = K^{1/v(r)} \qquad \textbf{Equation 2}$$

Equilibrium rate constants for most minerals in the system were adapted from the work by Xu et al. (2005 and 2007) with the following exceptions: Gudmundsson and Arnórsson (2005) for anoxic pyrite; and Gunnarsson and Arnórsson (2000) for amorphous silica. Augite was taken as an ideal solid solution between diopside and hedenbergite, but again using the values used by Xu et al. (2005 and 2007).

The summary of all chemical parameters can be found in Table 3.

2.4 Model Setup and Hydraulic Parameters

The experimental reactor was a titanium pressure vessel with a height of 15 cm and a radius of 0.625 cm. The same dimensions were applied to the rock sample volume. To provide better calculation resolution within the reactor model, the volume was divided into 200 blocks, with a fine block layer (0.00015 m) at the injection point, and another fine block layer at the production point (0.0015 m). The remaining layers were divided such that they were increasing in thickness logarithmically. The centre blocks were given a radius of 0.002286 m, with the remaining radial sections divided into logarithmically increasing thicknesses.

Pressure was maintained in the experiment using a back-pressure regulator. This same condition was modelled; however, the back-pressure process cannot be modelled by TOUGH2. Through iterative testing, it was found that a rock permeability value of 6.51 × 10-14 m^2 in all directions maintained the block pressures within the range of 35.67 to 35.68 bara for all runs.

Porosity was estimated based on the sample mass of 23.7 grams, the reactor volume and a New Zealand greywacke dry density of 2.6 g/cm3 (Hatherton & Leopard, 1964). The resulting value of 0.505 was used for the model.

The fluid injection was assigned to the bottommost block ' a20', while extraction was carried out from the topmost block ' a 1'. The flow rates used were either 1 mL or 0.5 mL (2.8 × 10-7 kg/s or 2.8 × 10-7 kg/s) to match the conditions used in the experiment.

Both porosity and permeability can be affected by the dissolution and precipitation of minerals within the reactor (and the numerical model). TOUGHREACT automatically calculates changes in porosity from the changes in individual mineral volume fractions and the specified molar volumes of each mineral in the thermodynamic database. On the other hand, parameters to account for the changes in permeability due to the changes in porosity need to be provided in the chemical.inp file. For this model, the simplified Carman-Kozeny relationship was selected for its ease of application.

2.5 Dilution Effect

It was reported by Passarella et al. (2015) that pure water leaked into the accumulator throughout the experiment. This was observed in the declining values of chloride, lithium and boron in the samples. To model the dilution, the water content in the boundary fluid (injectate) was adjusted throughout the model runs based on the measured chloride content.

Changing the water content created different fluid concentrations at each run day. This changing chemistry prevented the use of a single model that can calculate data for multiple days in a single run. Restart modelling was applied by capturing the SAVE and savechem files from one run and using them as the INCON and inchem data files, respectively, for the next data point's model. For more information on how to do this, refer to the TOUGHREACT Version 2.0 User's Guide by Xu et al. (2008).

2.6 Calibration

The general rate equation for the kinetic dissolution or precipitation of minerals is given by

$$r = k\left(\prod_1^m a_m^{n_m}\right)A\left|1-\Omega^{\theta}\right|^{\eta} \qquad \textbf{Equation 3}$$

In Equation 3, k is the mineral rate constant (dissolution or precipitation), a_m is the activity of the mth aqueous species (molals), n_m is the stoichiometry of the mth aqueous species, A is the reactive surface area (m^2/kg), Ω is the mineral saturation ratio, while θ and η are experimental rate constants (usually taken as equal to one) (Xu, 2008).

In TOUGHREACT, the reactive surface area of minerals is a function of several factors (Xu et al., 2008), but the most relevant to this study are V_{frac}, the mineral volume fraction ($m^3_{mineral}/m^3_{medium}$); A^0_m, the input mineral surface area ($m^2/m^3_{mineral}$); and r, the mineral radius (m).

In the process of calibration, only the A^0_m was used as the calibration parameter. Ultimately, the input mineral surface area values were specified iteratively to provide the best match for the sample chemistries.

Table 3: Rate constants, activation energies and rate laws for each mineral in the model system

Mineral	Acid Dissolution			Neutral		Other Dissolution			Precipitation			References
	$\log k_{25}$	E_a	Rate Law	$\log k_{25}$	E_a	$\log k_{25}$	E_a	Rate Law	$\log k_{25}$	E_a	Rate Law	
Pyrite				-4.55	56.9				6.42	-105.7	$\frac{a_{Fe^{2+}}a^2_{H_2S_{(aq)}}}{a_{H_2}a^2_{H^+}}$	Gudmundsson and Arnórsson (2005) Palandri & Kharaka (2004)
Calcite	-0.30	14.4	a_{H^+}	-5.81	23.5	-3.48	35.4	$a_{CO_{2(aq)}}$	-2.15	51.9	$a_{Ca^{2+}}a_{HCO_3^-}$	Xu et al. (2005 and 2007) Palandri & Kharaka (2004)
Magnesite	-6.38	14.4	a_{H^+}	-9.34	23.5	-5.22	62.8	$a_{CO_{2(aq)}}$	-8.05	91.5	$a_{Mg^{2+}}a_{HCO_3^-}$	Xu et al. (2005 and 2007) Palandri & Kharaka (2004)
Ca-Smectite				-12.78	35.0				26.73	-138.8	$a^{0.52}_{H_2O}a^{0.145}_{Ca^{2+}}a^{0.96}_{H^+}a^{0.26}_{Mg^{2+}}a^{3.97}_{SiO_{2(aq)}}a^{1.77}_{AlO_2^-}$	Xu et al. (2005 and 2007) Palandri & Kharaka (2004)
Augite	-6.82	78.0	$a^{0.7}_{H^+}$	-11.97	78.0							Xu et al. (2005 and 2007) Palandri & Kharaka (2004)
Chlorite	-11.11	88.0	$a^{0.5}_{H^+}$	-12.52	88.0							Xu et al. (2005 and 2007) Palandri & Kharaka (2004)
Illite	-3.66	46.0	$a^{0.6}_{H^+}$	-12.60	14.0	-0.57	67.0	$a^{0.6}_{OH^-}$				Xu et al. (2005 and 2007) Köhler et al. (2003)
Anhydrite				-3.19	14.3				1.11	60.2	$a_{Ca^{2+}}a_{SO_4{}^{2-}}$	Xu et al. (2005 and 2007) Palandri & Kharaka (2004)
Quartz				-13.99	87.7	-16.29	108366	$a^{0.5}_{H^+}$	-9.42	49.8	$a_{SiO_{2(aq)}}$	Xu et al. (2005 and 2007) Palandri & Kharaka (2004)
Amorphous Silica									-9.42	49.8	$a_{SiO_{2(aq)}}$	Gunnarsson and Arnórsson (2000) Palandri & Kharaka (2004)
Albite	-10.16	65.0	$a^{0.457}_{H^+}$	-12.56	69.8	-15.60	71.0	$a^{-0.572}_{H^+}$				Xu et al. (2005 and 2007) Palandri & Kharaka (2004)
K-Feldspar	-10.06	51.7	$a^{0.5}_{H^+}$	-12.41	38.0	-21.20	94.1	$a^{-0.823}_{H^+}$				Xu et al. (2005 and 2007) Palandri & Kharaka (2004)

3. MODEL RESULTS & DISCUSSION

3.1 Calibration Species

The main chemical species to which the model was calibrated to were Calcium, Magnesium, Iron, Aluminium, pH and Bicarbonate. Silica, Sodium and Potassium were treated as secondary calibration species, while Chloride, Sulphate, Lithium and Boron were considered as affected only by the dilution of the brine sample over time. Arsenic and Manganese were not included in the calibration. For each chemical species, corresponding calibration minerals were identified.

3.1.1 Calcium

Calcite can be used for quick calibration as it only produces Ca^{2+} and HCO_3^-, and directly affects pH. Multiple checks of the equilibrium constants have shown that the samples are undersaturated relative to calcite throughout the experiment, so it was decided to model the dissolution of calcite via kinetics. For calcite, the model input mineral surface areas were found to be four magnitudes smaller than the expected values for mineral RSA (reactive surface area) from White and Peterson (1990) or even those used by Xu et al. (2005 and 2007). It can be concluded from the relationship between input mineral surface area, the mineral volumetric function and the reactive surface area that the real fraction of calcite in the sample is significantly less than the initial value of 2.8%.

The second major contributor of calcium in the experiment is augite. For every mole of calcium released by augite, 0.75 moles of magnesium is also released. Because of this relationship, care was taken during the calibration to prevent an excess release of magnesium from augite. Calcium contributions from calcite and augite were balanced with losses due to the formation of Ca-smectite.

3.1.2 Magnesium

For most of the experimental data, magnesium contributions were accounted to both augite and chlorite. A simple form of chlorite was used for this model, only producing magnesium with silica, iron and aluminium. Chlorite was used to produce a background amount of magnesium, while augite was used to reproduce significant variations in magnesium concentrations.

There is, however, an exception to this approach which occurred between Data Points 11 and 20 during which time a disproportionate increase in magnesium was observed which did not coincide with an increase in calcium concentration. During this period, calibration of magnesium was done using magnesite, assumed as a small mineral pocket which completely dissolved away by the 21st experiment data point, at which point magnesium was again controlled only by chlorite, augite and smectite.

3.1.3 Iron

Iron was released from both augite and chlorite. Its low concentration in the resulting samples is due to its rapid consumption in the formation of pyrite. It was suggested by Passarella et al. (2015) that the formation occurs rapidly under equilibrium conditions. During modelling, it was found that the reaction did occur rapidly and approached equilibrium closely but not exactly. It occurred quickly enough that the input mineral surface areas required to match the iron concentrations are only between 1.0×10^{-8} and 3.1×10^{-6} m^2/m^3.

This rapid reaction rate created modelling issues. The closer the modelled kinetics is to equilibrium, the more time and time steps TOUGHREACT needed to reach convergence. This issue was resolved by shifting the equilibrium constants up by a fixed log constant value which corresponds with the final kinetic conditions during the second half of the experiment and changing the mechanism to equilibrium. As a result, the first part of experimental results was modelled kinetically, while the later parts were modelled under equilibrium, corresponding to kinetics that are closer to equilibrium. The pseudo-equilibrium constants used are shown in Figure 3.

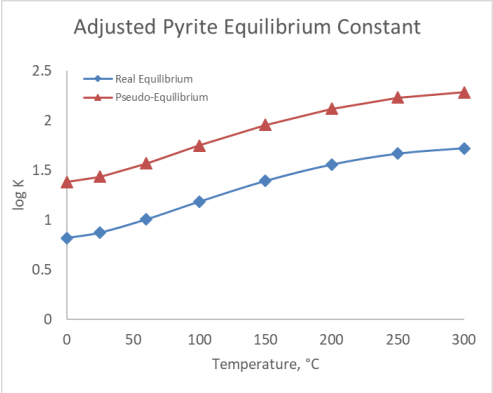

Figure 3: Adjusted equilibrium constants for pyrite used to model near equilibrium kinetics.

3.1.4 Aluminium

The final concentration of aluminium was calibrated using smectite.

3.1.5 pH and Bicarbonate

The experimental pH was affected in two ways – (1) by the direct consumption or production of H+ from the dissolution and precipitation reactions; and (2) from the release of bicarbonate from carbonate mineral dissolution and consumption of hydrogen sulphide in pyrite formation, and their subsequent equilibration. The overall effect of the fluid-rock interaction is to raise the pH as there are more reactions which tended to increase the pH, in agreement with experimental conditions.

More emphasis was given to bicarbonate matching compared to pH, with specific adjustments performed using calcite.

3.1.6 Sodium and Potassium

Sodium in the experiment can be released by albite, while potassium can be released from k-feldspar and illite. However, the modelling calibrations showed that all three minerals were supersaturated and so no dissolution occurs.

3.1.7 Silica

Silica can be released by augite, chlorite, illite, albite and k-feldspar. It is consumed by the formation of smectite. Like pH, silica content was considered as a secondary effect of matching the other species in the experiment.

An attempt was made to match the silica via the formation of quartz. Using an A^0_m value of 3.2×10^4 m^2/m^3, the silica content was modelled to within 30 ppm of experimental data with marginal effect to the calibrated values for pH, calcium and magnesium (< 0.05 unit). It had the beneficial effect of raising the modelled aluminium concentration in the second half of the experiment closer to measured values. This single value was observed to provide a consistent match throughout the entire model. However, it was not applied to the final model as secondary quartz was not reported to have been observed in the study by Passarella et al. (2015).

Amorphous silica, on the other hand, was found to be undersaturated throughout the experiment, so was not expected to form.

3.2 Reactive Surface Area

In the process of calibration, the input mineral surface area values were allowed to vary to provide the best match to the experimental chemistry. The log values of the A^0_m are presented in Figure 4 for the reactive minerals.

Both pyrite and smectite were found to have increasing reactive surface areas at the beginning of the experiment. It is assumed that at the start of the deposition of either mineral, heterogeneous nucleation is occurring slowly. As the reaction progresses, the crystal nuclei grow, increasing the surface area to which more crystals can attach. This occurred until a stable surface area was reached for both minerals.

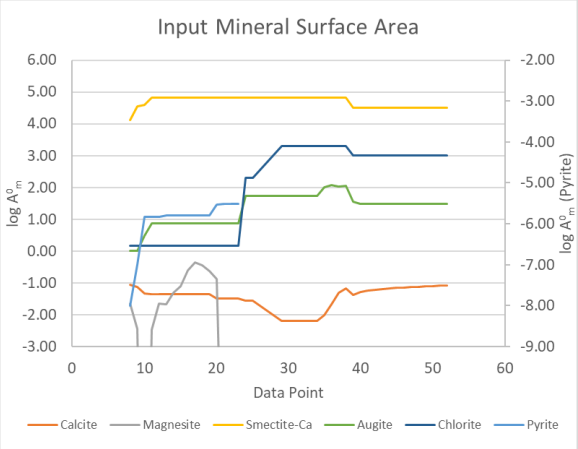

Figure 4: Input mineral surface areas from model calibration for reactive minerals.

Reactive surface areas for both augite and chlorite were found to be increasing as the experiment progressed. According to Pollet-Villard et al. (2016), etch pits generally formed during mineral dissolution. Upon the formation of etch pits, mineral surface areas increase, subsequently increasing the mineral reaction rate. These etch pits were observed under SEM analysis by Passarella et al. (2015). Photographs showing the etch pits can be seen in Figure 5.

Calcite was observed to decrease in RSA from the start of the experiment until Data Point 34. In this period, the originally exposed calcite is slowly getting dissolved away, causing a successive reduction in its surface area. However, after Data Point 35 calcite RSA began increasing again. This increase accounts for the continuous rise in calcium concentration in the samples without any accompanying increase in the magnesium and aluminium concentrations. It is hypothesised that the dissolution of both augite and chlorite exposed previously inaccessible grains of calcite, causing the increase in RSA.

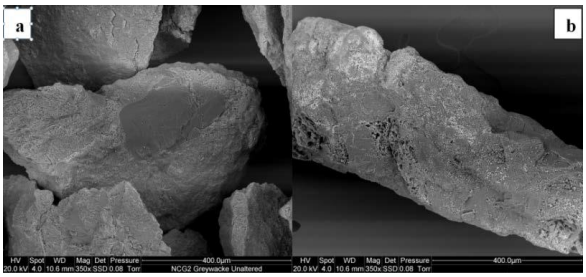

Figure 5: Photographs of an (a) unreacted greywacke grain sample and (b) heavily corroded ferromagnesian minerals on a greywacke grain, showing the etch pits. Bright spots in (b) are pyrite crystals. Reprinted from Passarella et al. (2015).

It is also notable that the A^0_m dips at Data Point 39. This was intentionally modelled as an effect of the reduction in reactor flowrate. In their study, Kieffer et al. (1999) observed that at low flow rates, increasing the bulk flow rate in flow-through reactors caused an increase in the reactive surface area of their sandstone substrate. They explained that the most likely reason is the build-up of pore pressure at higher flow rates. In the case of the experiment by GNS, as the reactor outlet pressure is controlled at a fixed value, it is expected that more pressure is needed at the inlet when injecting 1 mL/hr of fluid compared to 0.5 mL/hr. The corresponding increase in pore pressure can in effect widen or create new pore channels, increasing the reactive surface area. As the inverse was done during the experiment, the RSA was expected to decrease with the flow reduction.

3.3 Results

The reactor model results are shown in Figures 6 to 11. Figures 6 and 7 present the model outputs for chloride, and sodium. As discussed in section 2.5, the brine reactant was diluted by distilled water ingress into the accumulator apparatus. This was modelled using the chloride concentration as a basis. It is apparent from 6 and 7 that chloride and sodium were conservative; the same behavior was observed for lithium, boron and potassium.

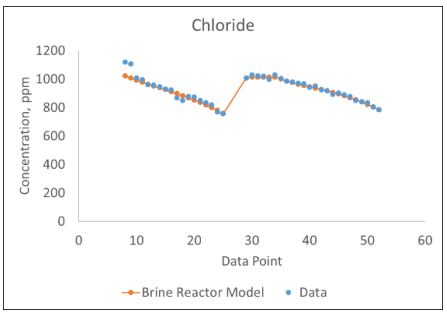

Figure 6: Model chemistry outputs from the Brine Reactor Model for chloride.

Bicarbonate was closely matched for the first half of the experiment, as can be seen in Figure 8, but the model produced values higher than the experimental data for the second half of the experiment. This divergence was accepted as it still follows the trend in bicarbonate concentration, and

allowed for closer calibration of calcium, magnesium and pH.

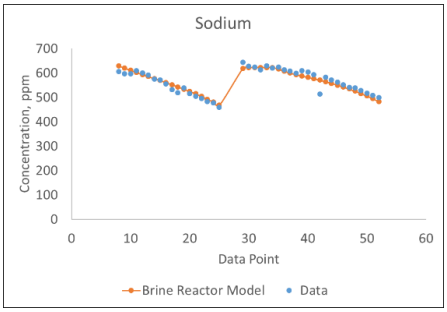

Figure 7: Model chemistry outputs from the Brine Reactor Model for sodium.

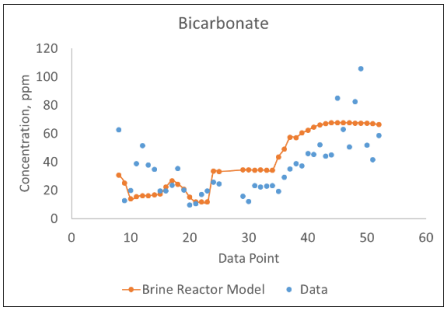

Figure 8: Model chemistry outputs from the Brine Reactor Model for bicarbonate.

Figure 9 shows the output for pH. pH was not as critically matched as other chemical species in the experiment. Despite this, the increasing trend of pH over time has been captured.

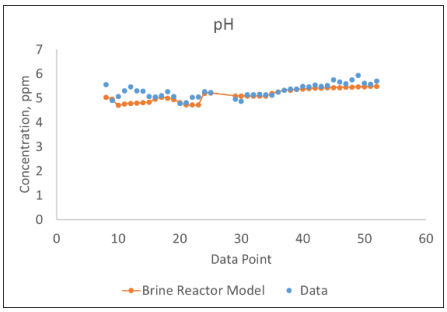

Figure 9: Model chemistry outputs from the Brine Reactor Model for pH.

Figure 10 shows the match done for calcium. Matching was performed through calcite, augite and Ca-smectite modelling. Calcium was treated as a primary calibration species which accounts for the high level of agreement with experimental data. A high degree of match was also achieved for magnesium. The calibration for iron captured the initial slower precipitation rate of pyrite, as well as the approach of the reaction to equilibrium.

Hydrogen sulphide was not satisfactorily matched as shown in Figure 11. The model was partially able to match the concentration trend behaviour over time, but on average produced concentration values exceeding the experiment data by 25 ppm. In the system, the precipitation of pyrite consumes the greatest amount of H_2S, with minor contributions from the dissociation due to pH. An alternative calibration method was tested which involved increasing the dissolution rate of augite to produce more ferrous ions. This caused a decrease in hydrogen sulphide concentration to 72 ppm relative to 68 ppm from the experiment; however, it also caused the pH to overshoot by 0.38 and the bicarbonate concentration to go as high as 136 ppm. It is for this reason that the assumptions of the final model were accepted despite the non-convergence relative to hydrogen sulphide.

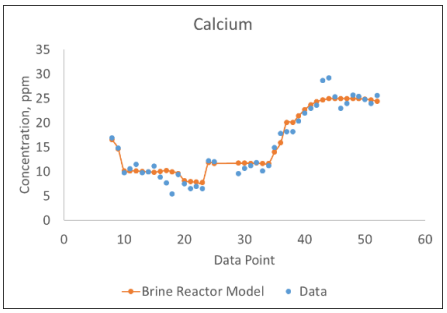

Figure 10: Model chemistry outputs from the Brine Reactor Model for calcium.

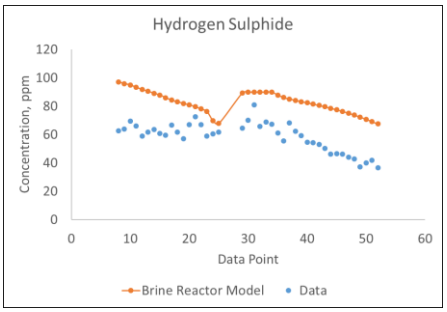

Figure 11: Model chemistry outputs from the Brine Reactor Model for hydrogen sulphide.

Both porosity and permeability increase as a result of mineral dissolution, and are decreased by precipitation. In the brine reactor model, the predominant process is dissolution. The largest contributors to mineral dissolution are augite and calcite, followed by chlorite.

Similarly, the precipitation of both pyrite and Ca-smectite occur in higher rates in the first sections of the reactor. It was noted that the net change is a loss in mineral volume, with the maximum loss expected at the reactor inlet. As a result, both porosity and permeability increased in the model (Figure 12). The peak permeability and porosity effects are expected at the reactor inlet, coinciding with the location of maximum material loss. The porosity changes range from +0.0007 to +0.0021, while permeability changes range from $+0.04 \times 10^{-14}$ m^2 to $+0.14 \times 10^{-14}$ m^2.

For comparison, the effect of injecting only the de-oxygenated brine was modelled. With the exception of not including the NCGs in the fluid chemistry parameters, the model was set-up the same way as the brine-NCG model, and all values for A^0_m from the brine model calibration were retained.

Figure 13 shows permeability and porosity effects without NCG. The dissolution of the primary minerals is offset by the formation of Ca-smectite, leading to an overall decrease in both porosity and permeability. Pyrite neither dissolved nor precipitated to a significant degree due to the absence of both H_2 and H_2S. The results indicate that the addition of NCG to brine injectate reverses the effect of injecting pure brine to a

significant degree, shifting the reaction from an overall net deposition to a net dissolution.

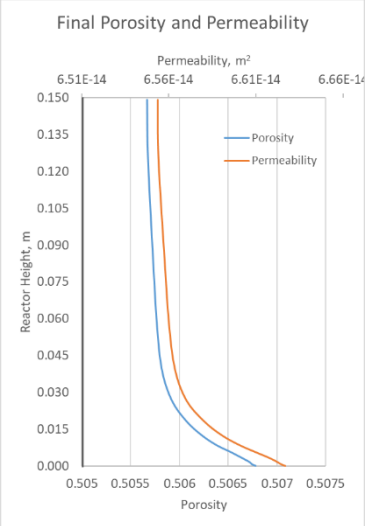

Figure 12: Plot of modelled greywacke porosity and permeability at the end of the experiment (original values marked by dark grey line).

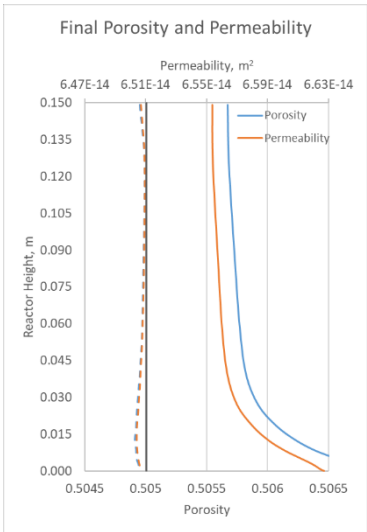

Figure 13: Comparative plot of modelled greywacke porosity and permeability at the end of the experiment with brine-NCG (solid lines) and brine (broken lines), original values marked by a dark grey line.

4. SUMMARY AND CONCLUSIONS

This research was able to meet its objective of modelling the brine-greywacke experiment conducted by GNS Science in 2015. The TOUGHREACT software proved to be a highly robust tool for modelling fluid-rock interactions in a variety of chemical process conditions and can provide insights into the evolution of local geologic structures in the presence of a variety of fluid injectates.

Sufficient agreement between experimental data and model values were observed after calibration. Through calibration, it was discovered that the reactive surface areas of minerals evolve with the progression of dissolution and do not necessarily follow the spherical grain model for minerals. The formation of etch pits during the dissolution process was found to increase the surface areas and reaction rates over time, leading to fluctuations in fluid chemistry.

The evolution of surface areas is an important consideration for future modelling efforts. However, the unpredictable nature of the evolution provides modelling complexity. It is recommended that laboratory experiments be run for longer durations until final stable reactive surface area values for each mineral are achieved.

The effect of fluid flow rate to the effective mineral reactive surface area should be considered. It was observed that the effective reactive surface area decreased when the injection flow rate was reduced. What this implies is that the injection flow rate has an effect on the dissolution and precipitation rates of minerals and may have applications for controlling the permeability and porosity effects of injection in actual field scenarios.

It was shown that the addition of NCGs decreased the pH of injectates. This decrease in pH promotes mineral dissolution, which subsequently increases rock porosity and permeability. Brines are generally supersaturated relative to minerals and prevent dissolution of primary mineralogy while promoting deposition of secondary minerals. This was modelled to lead to a general loss of porosity and permeability. The addition of NCG was found to promote the dissolution of minerals. As a result, the addition of NCG is expected to cause a significant improvement in porosity and permeability over time.

The porosity and permeability changes indicate the viability of reservoir stimulation through the co-injection of NCG with injectates. However, these experiment and models show little evidence of CO_2 sequestration. On the other hand, H_2S was shown to be fixed as pyrite. Considering the small scale of the reactor system, this observation is not necessarily conclusive. It is recommended that a larger scale model is developed based on the calibrated model to evaluate if further deposition of carbonate minerals can occur at distances further away from the injection point. Similar behaviours have been documented in the models by Xu et al. (2007 and 2007).

Finally, it is recommended that future studies be conducted on wellbore and reservoir models incorporating the findings from this work.

ACKNOWLEDGMENTS

The authors would like to express their gratitude to Dr Bruce Mountain and Dr Mauro Passarella of GNS Science for their valuable inputs and research without which this work would not have been possible.

The authors would like to express appreciation as well for Dr Bridget Lynne of the University of Auckland for providing additional geoscientific inputs and for challenging assumptions and results.

REFERENCES

Doughty, C., Pruess, K., Benson, S. M., Hovorka, S. D., Knox, P. R., & Green, C. T. (2001). Capacity investigation of brine-bearing sands of the Frio formation for geologic sequestration of CO2. Retrieved from http://digital.library.unt.edu/ark:/67531/metadc723873/

Fridriksson, T., Mateos, A., Audinet, P., & Orucu, Y. (2016). Greenhouse Gases from Geothermal Power Production. World Bank, Washington, DC.

Gudmundsson, B. T., & Arnórsson, S. (2005). Secondary mineral–fluid equilibria in the Krafla and Námafjall geothermal systems, Iceland doi://doi.org/10.1016/j.apgeochem.2005.04.020

Gunnarsson, I., & Arnórsson, S. (2000). Amorphous silica solubility and the thermodynamic properties of H4SiO°4 in the range of 0° to 350°C at Psat doi://doi-org.ezproxy.auckland.ac.nz/10.1016/S0016-7037(99)00426-3

Hatherton, T., & Leopard, A. E. (1964). The densities of New Zealand rocks. New Zealand Journal of Geology and Geophysics, 7(3), 605-625. doi:10.1080/00288306.1964.10422108

Horiuti, J. (1957). In Farkas A. (Ed.), 35 A Theorem on the Relation between Rate Constants and Equilibrium Constant Academic Press. doi://doi-org.ezproxy.auckland.ac.nz/10.1016/S0360-0564(08)60183-2

Kaszuba, J. P., Janecky, D. R., & Snow, M. G. (2003). Carbon dioxide reaction processes in a model brine aquifer at 200 °C and 200 bars: implications for geologic sequestration of carbon doi://doi-org.ezproxy.auckland.ac.nz/10.1016/S0883-2927(02)00239-1

Kaya, E., & Zarrouk, S. J. (2017). Reinjection of greenhouse gases into geothermal reservoirs doi://doi-org.ezproxy.auckland.ac.nz/10.1016/j.ijggc.2017.10.015

Kieffer, B., Jové, C. F., Oelkers, E. H., & Schott, J. (1999). An experimental study of the reactive surface area of the Fontainebleau sandstone as a function of porosity, permeability, and fluid flow rate doi://doi-org.ezproxy.auckland.ac.nz/10.1016/S0016-7037(99)00191-X

Knauss, K. G., Johnson, J. W., & Steefel, C. I. (2005). Evaluation of the impact of CO2, co-contaminant gas, aqueous fluid and reservoir rock interactions on the geologic sequestration of CO2 doi://doi-org.ezproxy.auckland.ac.nz/10.1016/j.chemgeo.2004.12.017

Lawrence Berkeley National Laboratory. (2018). TOUGHREACT Software. Retrieved from http://esd1.lbl.gov/research/projects/tough/software/toughreact.html

McIntyre, J., Berg, B., Seto, H., & Borchardt, S. (2011). Comparison of Lifecycle Greenhouse Gas Emissions of Various Electricity Generation Sources.

NASA Jet Propulsion Laboratory. Global surface temperature | NASA Global Climate Change. Retrieved Jun 19, 2018, from https://climate.nasa.gov/vital-signs/global-temperature

Palandri, J. L., & Kharaka, Y. K. (2004). A Compilation of Rate Parameters of Water-Mineral Interaction Kinetics for Application to Geochemical Modeling.

Passarella, M., Mountain, B., Zarrouk, S., & Burnell, J. (November 18, 2015). EXPERIMENTAL SIMULATION OF RE-INJECTION OF NON-CONDENSABLE GASES INTO GEOTHERMAL RESERVOIRS: GREYWACKE-FLUID INTERACTION. Paper presented at the 37th New

Pollet-Villard, M., Daval, D., Fritz, B., Knauss, K. G., Schäfer, G., & Ackerer, P. (2016). Influence of etch pit development on the surface area and dissolution kinetics of the orthoclase (001) surface. Chemical Geology, 447, 79-92. doi:10.1016/j.chemgeo.2016.09.038

Solomon, S., Plattner, G., Knutti, R., & Friedlingstein, P. (2009). Irreversible climate change due to carbon dioxide emissions. Proceedings of the National Academy of Sciences, 106(6), 1704-1709. doi:10.1073/pnas.0812721106

Stats, N. Z. (2018). Global greenhouse gas emissions. Retrieved from http://archive.stats.govt.nz/browse_for_stats/environment/environmental-reporting-series/environmental-indicators/Home/Atmosphere-and-climate/global-greenhouse-gases.aspx

White, A. F., & Peterson, M. L. (1990). Role of Reactive-Surface-Area Characterization in Geochemical Kinetic Models. Chemical Modeling of Aqueous Systems II (pp. 461-475) American Chemical Society. doi:10.1021/bk-1990-0416.ch035

Xu, T., Apps, J. A., & Pruess, K. (2005). Mineral sequestration of carbon dioxide in a sandstone–shale system doi://doi-org.ezproxy.auckland.ac.nz/10.1016/j.chemgeo.2004.12.015

Xu, T., Apps, J. A., Pruess, K., & Yamamoto, H. (2007). Numerical modeling of injection and mineral trapping of CO2 with H2S and SO2 in a sandstone formation doi://doi-org.ezproxy.auckland.ac.nz/10.1016/j.chemgeo.2007.03.022

Xu, T., Spycher, N., Sonnenthal, E., Zheng, L. and Pruess, K. (2012). TOUGHREACT User's Guide: A Simulation Program for Non-isothermal Multiphase Reactive Transport in Variable Saturated Geologic Media, Version 2.0. Retrieved from https://www.researchgate.net/publication/255003632_TOUGHREACT_User%27s_Guide_A_Simulation_Program_for_Non-isothermal_Multiphase_Reactive_geochemical_Transport_in_Variable_Saturated_Geologic_Media